# Combinatorial immunophenotyping of cell populations with an electronic antibody microarray

*Ruxiu Liu,[a] Chia-Heng Chu,[a] Ningquan Wang,[a] Tevhide Ozkaya-Ahmadov,[a] Ozgun Civelekoglu,[a] Dohwan Lee,[a] A K M Arifuzzman,[a] A. Fatih Sarioglu*[*abc]

[a] School of Electrical and Computer Engineering, Georgia Institute of Technology, Atlanta, GA 30332, United States
[b] Parker H. Petit Institute for Bioengineering and Bioscience, Georgia Institute of Technology, Atlanta, GA 30332, United States
[c] Institute for Electronics and Nanotechnology, Georgia Institute of Technology, Atlanta, GA 30332, United States
E-mail: sarioglu@gatech.edu

Keywords: microfluidics, microarray, immunophenotyping, flow cytometry, complete blood count

Immunophenotyping is widely used to characterize cell populations in basic research and to diagnose diseases from surface biomarkers in the clinic. This process usually requires complex instruments such as flow cytometers or fluorescence microscopes, which are typically housed in centralized laboratories. We combine microfluidics with an integrated electrical sensor network to create an antibody microarray for label-free cell immunophenotyping against multiple antigens. Our device works by fractionating the sample via capturing target subpopulations in an array of microfluidic chambers functionalized against different antigens and by electrically quantifying the cell capture statistics through a network of code-multiplexed electrical sensors. Through a combinatorial arrangement of antibody sequences along different microfluidic paths, our device can measure the prevalence of different cell subpopulations in a sample from computational analysis of the electrical output signal. We characterize the device performance by analyzing heterogeneous samples of mixed tumor cell populations and then apply our technique to determine leukocyte subpopulations in blood samples and validate our results against complete blood cell count and flow cytometry results. Label-free immunophenotyping of cell populations against

multiple targets on a disposable electronic chip presents opportunities in global health and telemedicine applications for cell-based diagnostics and health monitoring.

## 1. Introduction

Cell surface markers are essential proteins or carbohydrates[1,2] involved in a variety of cell functions, ranging from cell-cell interactions, ligand-receptor binding, and cell signaling, to serving as transporters, ion channels, enzymes, and adhesion molecules.[3] Because different cell types usually express varying subsets of surface markers, cell surface markers, especially cluster of differentiation (CD) antigens,[4] serve as chemical fingerprints to identify and classify cells (e.g., CD8 is a marker for cytotoxic T cell, a type of cancer-killer cell in the human immune system).[5] Moreover, the expression of cell surface markers is dynamically altered at different stages during the differentiation of cell lineages, both for healthy cells and malignant tumor cells. For example, CD43 is expressed on the later stages of B cells but not on the earlier stages;[6] the carcinoembryonic antigen (CEA) is highly correlated to the development of colorectal cancer.[7] The profiling of the cell surface markers, i.e., immunophenotyping, is, therefore, an important process with a wide range of applications in basic research and clinical studies to provide comprehensive information about the cell state, and is routinely used to characterize cells in lineages of differentiation and to diagnose and classify diseases derived from those cells.

Currently, the gold standard for immunophenotyping assays is the flow cytometry, which can optically interrogate cells for target antigens.[8] In flow cytometry, cells have to be first labeled with fluorophore-conjugated antibodies specifically targeting antigens of interest. Fluorescently labeled cells are then interrogated one by one as they flow through a detection zone, where fluorophores are excited by lasers, and the resulting fluorescence emission is

measured by an array of photodetectors. From the fluorescence intensity, flow cytometers can quantify surface marker expression on cells and are therefore widely used for cell profiling in various research and clinical applications.[9-15] On the other hand, a flow cytometer is usually limited in the number of antigens it can simultaneously probe due to overlap between excitation and emission spectra of different fluorophores.[3,16] Moreover, flow cytometry cannot be performed at the point of care and has limited adoption beyond centralized laboratories due to bulky and expensive instrumentation that requires trained operators.

Microfluidic devices have also been used as immunoassays that can deterministically screen cell populations in a well-controlled microenvironment. Such devices rely on highly specific immunoaffinity-based capture of cells expressing target antigens and can be used to identify subpopulations in a microarray format.[17-23] However, these assays mostly require external instrumentation such as a microscope for the readout, which negates the cost and portability benefits of the microfluidic chip itself. Standalone lab-on-a-chip assays that can quantitatively analyze cells can be built by integrating sensors into the microfluidic chip. Among various types of biosensors, Coulter counters[24,25] are particularly attractive as they provide robust on-chip detection using simple electrodes that can easily be integrated into a microfluidic device. In fact, Coulter counters have been previously employed to quantify immunocapture of cells in a microfluidic chip by differentially counting cells at the inlet and outlet of the device.[26-29] While providing an integrated solution, existing approaches are limited in their scalability to screen against multiple antibodies due to challenges (1) in integrating a large number of electrical sensors into the device without increasing device complexity and (2) in selective functionalization of different parts of the microfluidic device to create a multiplexed microarray format.

In this paper, we introduce a microfluidic antibody microarray, whose results are acquired by an integrated electrical sensor network. Our microfluidic device consists of an array of microfluidic cell capture chambers, each functionalized with a different antibody to recognize a target antigen, and a network of code-multiplexed Coulter counters placed at strategic nodes across the device to quantify the fraction of cell population captured in each microfluidic chamber (**Figure** 1a). With our technique, we interpret the electrical data providing cell capture statistics across the device in light of the specific antibody sequence each cell was subjected to, for calculating the prevalence of different subpopulations in a sample. Moreover, by electrically coding cell capture data, we compress the cell capture statistics across the whole device into a single electrical output without any information loss. We first demonstrate the device operation on a mixed population of different tumor cells. Then, we apply our technique for identifying leukocyte subpopulations in a blood sample and benchmark our results against flow cytometry and a hematology analyzer on matched samples.

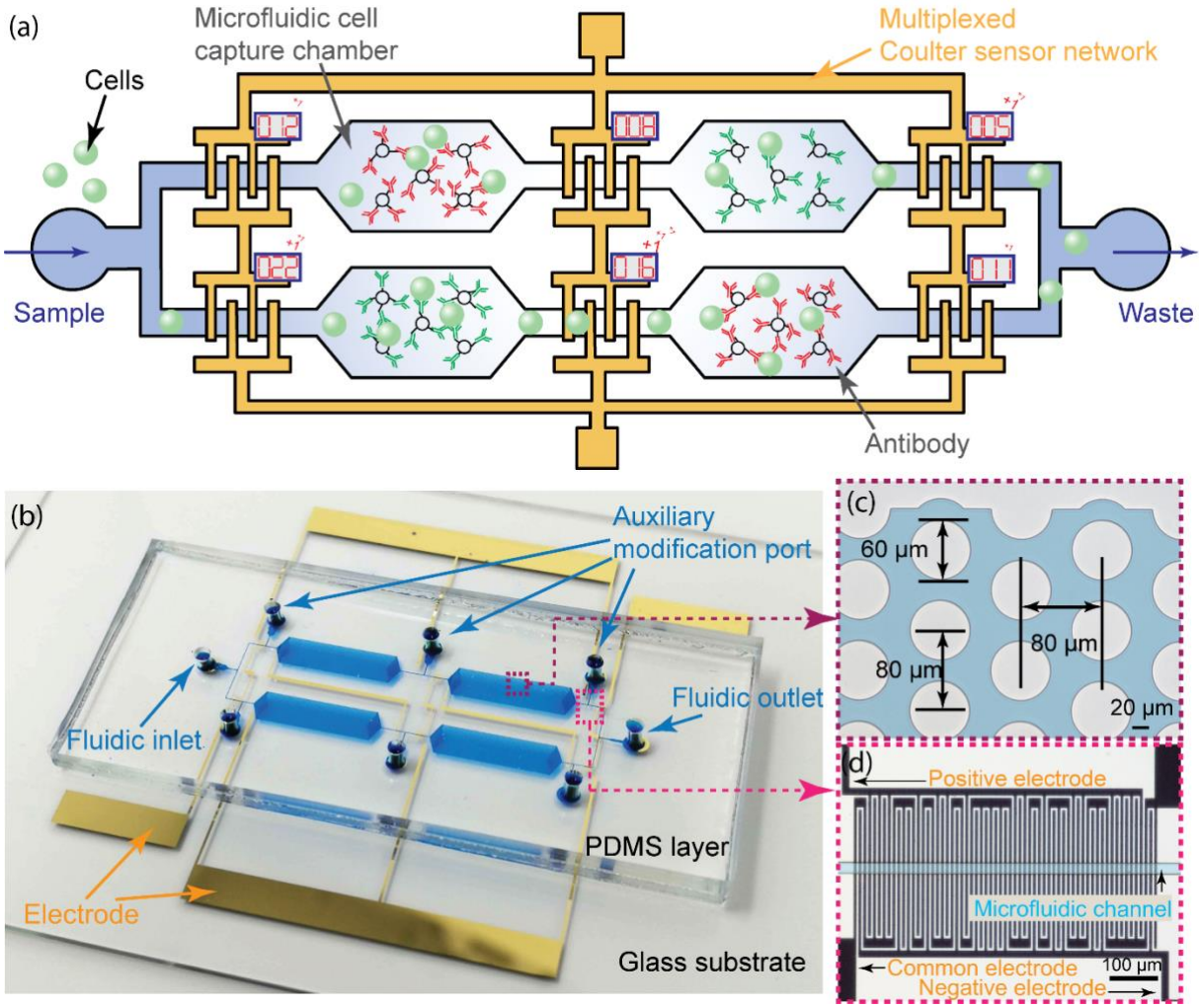


**Figure 1.** The operation principle and the design of the electronic antibody microarray. (a) A schematic showing the operation of the device. Each microfluidic cell capture chamber is functionalized with a different antibody. Cells expressing the target antigen are immunocaptured in the microfluidic chambers. The number of captured cells in each chamber is determined by an on-chip network of electrical sensors placed at strategic nodes across the device. (b) A photo of the fabricated device filled with blue dye for illustration. The fabricated device is made up of a PDMS layer with microfluidic channels and cell capture chambers, and a glass substrate with a micropatterned metal layer forming the sensor network. Besides the sample inlet and outlet, auxiliary ports were created on the microfluidic layer for selective functionalization of individual cell capture chambers. (c) A close-up image of the cell capture chamber. 60 µm-diameter pillars are arranged in a staggered array with an 80 µm-pitch, to enhance the cell capture rate. The channel is filled with a blue dye for visualization purposes. (d) A close-up image of one of the electrical sensors on the device. The sensor is specifically designed to form an electrode pattern to produce a 31-bit digital code (0111001011010000110100110011110), each time a cell flows over it. Other sensors are coded with different orthogonal codes enabling a code-multiplexed readout shared by all sensors.

## 2. Results and discussion

### 2.1. Device design and operation

We designed and fabricated a two by two microfluidic antibody microarray with an electrical readout as a proof of concept (**Figure** 1b). Our device is composed of a polydimethylsiloxane (PDMS) microfluidic layer that accommodates the cell capture chambers (**Figure** 1c) and a glass substrate with a code-multiplexed Coulter sensor network made up of micropatterned gold electrodes (**Figure** 1d). In the microfluidic layer, the sample inlet bifurcates into two separate microfluidic paths, with each path consisting of two cascaded cell capture chambers. In both microfluidic paths, cells sequentially interact with two different antibodies immobilized in the microfluidic chambers before all cells are merged and discharged from the waste outlet. Code-multiplexed Coulter sensors log each and every cell as the cell enters the device if it passes from one capture chamber to another, and if it gets discharged from the device, to determine the antigen-positive cell count in each cell capture chamber from a mass balance calculation.

In our device, microfluidic cell capture chambers replace antibody spots in a conventional assay and are designed to efficiently capture the cells expressing target surface antigens. Each cell capture chamber measures 9 mm in length and 3 mm in width. Within each cell capture chamber, we placed 60 μm-diameter pillars to increase the cell capture area and to structurally support the cell capture chamber ceiling (**Figure** 1c). The pillars form a staggered two-dimensional array with an 80 μm-pitch to increase the likelihood of cell-pillar contact under laminar flow. To selectively modify each chamber with a specific antibody, we added a set of auxiliary functionalization ports in the PDMS layer. These auxiliary ports are located close to the inlet and outlet of each cell capture chamber (**Figure** 1b), to exclusively deliver the functionalization reagents to the desired cell capture chamber. Following the functionalization

process, auxiliary ports were sealed to prevent leakage during the assay, and the device was interfaced via a single fluidic inlet and outlet.

To functionalize cell capture chambers with antibodies, we employed a four-step chemical modification protocol (Experimental Section, *Immobilization of antibodies in the microfluidic device*). To selectively immobilize different antibodies in the intended cell capture chambers, we used auxiliary functionalization ports. In this process, capture antibodies for different cell capture chambers were simultaneously introduced into the device through their dedicated functionalization ports at the same flow rate (**Figure** 2a(i)). Simultaneous injection of antibody solutions through symmetrically designed microfluidic paths combined with the laminarity of the flow ensured that each antibody is exclusively directed into the desired cell capture chamber without mixing with others. To minimize antibody loss from the waste ports in this process, Tygon tubes were employed to increase the hydraulic resistance of the waste path diverting most (>80%) of the solution into the capture chambers. The characterization of this concurrent functionalization approach using different colored dyes demonstrated its effectiveness with no observable crosstalk between different cell capture chambers (**Figure** 2b). While the diffusion across different cell capture chambers during incubation may induce mixing, the distance between different chambers makes its effect negligible in the functionalization of cell capture chambers. The main advantages of our approach over the printing-based deposition of antibodies[3] are twofold: First, we can perform the whole functionalization process in a closed chamber without exposing the antibodies to the ambient during buffer exchanges. Second, we functionalize all inner surfaces of the microfluidic chambers, which enhances capture efficiency. It should also be noted that except for the antibodies, auxiliary functionalization ports were used as outlets in the functionalization process for applying reagents common to all cell capture chambers ((3-

aminopropyl)triethoxysilane (APTES) and glutaraldehyde) (**Figure** 2a(ii)). Once the functionalization process was completed, all auxiliary functionalization ports were sealed, the sample was introduced to the device from a common inlet, and the waste was discharged from the common outlet (**Figure** 2a(iii) and 3a). Overall, our functionalization process utilizes the same chemistry employed for preparing immunoassays and can also be scaled to create larger assays with more antibodies.

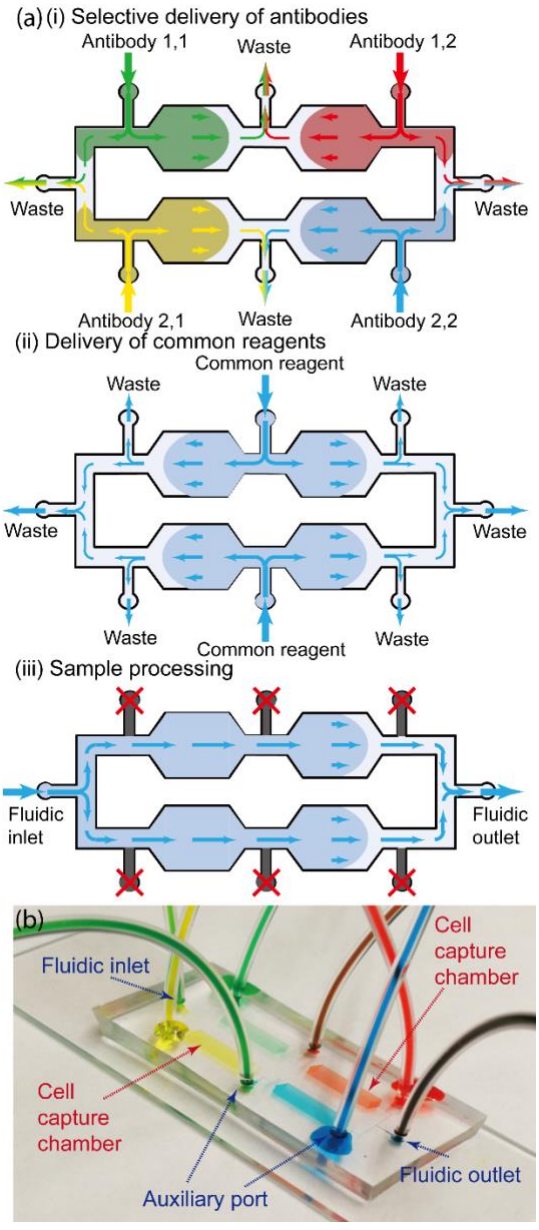

**Figure 2.** Functionalization of the cell capture chambers. (a) Computer drawings depicting different schemes for interfacing the device for surface functionalization and sample processing. (i) All four antibodies are simultaneously introduced from the auxiliary functionalization ports to specifically deliver the capture antibodies to the desired cell capture chamber. The laminar flow combined with the symmetric device design prevents any mixing between different antibody solutions. (ii) The buffers and reagents common to all cell capture chambers are introduced from an inlet and the auxiliary functionalization ports operate as outlets. (iii) Prior to sample processing, auxiliary functionalization ports are sealed. The sample is then introduced from a single inlet and the waste is collected from a single outlet. (b) A photo of a device, where four different solutions each containing a different colored dye could successfully be delivered to individual cell capture chambers using the developed process. Lack of mixing between different colors demonstrates the capability to specifically deliver different antibodies to corresponding microfluidic chambers.

To electrically measure the number of captured cells in each of the functionalized cell capture chambers, we employed a network of coded Coulter sensors distributed across the device. Our sensing strategy is based on the Microfluidic CODES scheme, which uses micromachined electrode patterns to multiplex spatiotemporal cell data across a microfluidic device.[30-32] In our device, a three-electrode Coulter counter was shaped to form distinct electrode patterns (i.e., sensors) at six different nodes to monitor cell passage between microfluidic chambers. Each sensor is composed of an array of 5 μm-wide finger electrodes separated by 5 μm gaps and produces a specific 31-bit digital code, which was implemented by an interdigitated arrangement of three electrodes: two sensing electrodes to set the bit polarity (positive for “1” and negative for “0”) and one common electrode meandering in between to excite the sensor network (**Figure** 1d). Cells flowing over one of these sensors sequentially modulated the local impedance between adjacent finger electrodes via the Coulter principle and generated a distinct bipolar electrical waveform dictated by the surface electrode pattern. In addition, we designed sensor codes to be mutually orthogonal (Gold sequences),[33,34] and therefore, we could (1) reliably discriminate sensor signals from each other in the output signal and (2) resolve interfering signals when multiple cells are coincidentally detected by the same or different sensors (**Table** 1.1).[30,32] Moreover, in the case of cell debris or aggregates, the

electrical signal generated by sensors do not match any of the templates constructed based on single cell signals and therefore, these data are discarded and do not affect the assay performance.

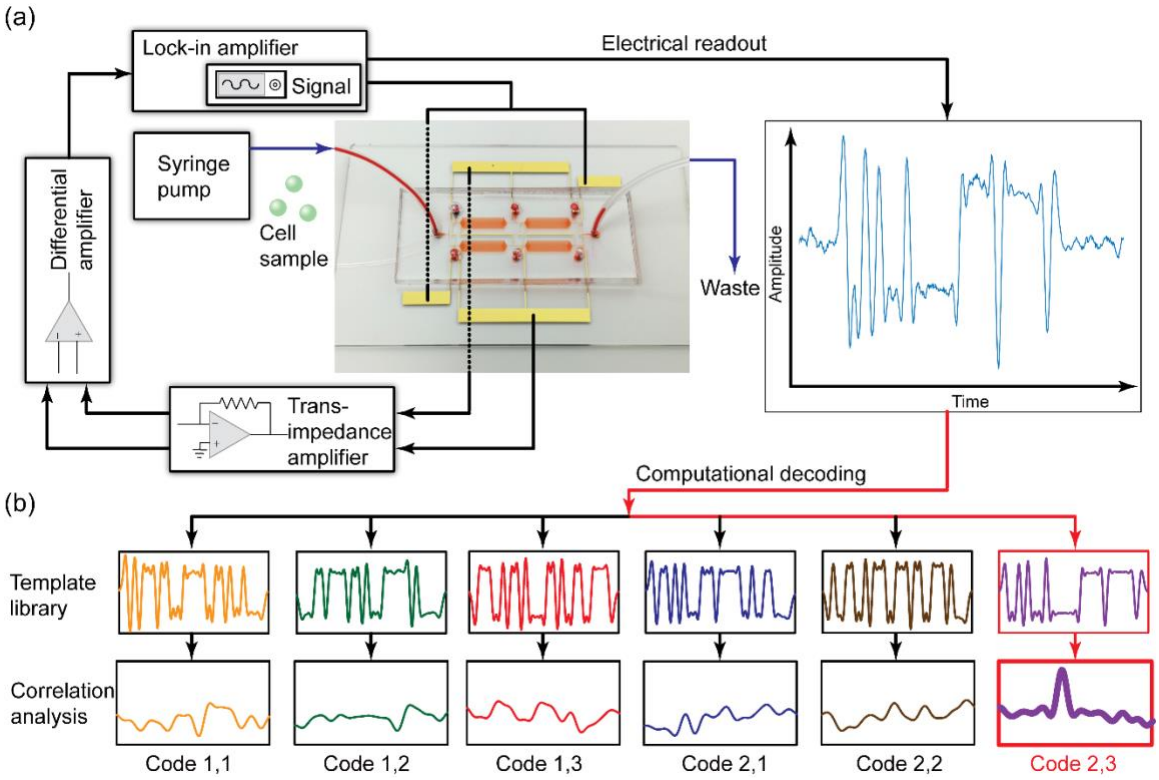


**Figure 3.** The electrical acquisition of the cell capture statistics across the antibody microarray. (a) A schematic of the experimental setup used for the sample delivery and electrical measurements. Cells are driven through the device at a constant flow rate with a syringe pump. The electrical sensor network is excited using a sine wave generated from the lock-in amplifier, and the resulting current signal is first converted to voltage signals using transimpedance amplifiers, then subtracted from each other by a differential amplifier and the signal amplitude is measured using a lock-in amplifier. (b) The decoding process to identify individual sensor signals in the device output signal. The output signal is correlated with a template library consisting of signature waveforms corresponding to each and every coded sensor in the network using a custom-built algorithm. A correlation peak is used to identify the matching template and the specific sensor that detected the cell. The specific case in the figure demonstrates the decoding of a signal produced by the sensor with the Code 2,3.

During the assay, the sample was driven through the functionalized device by a syringe pump at a controlled flow rate and followed by a brief phosphate buffered saline (PBS) wash to clear the device of remaining cells. The electrical signal from the device was acquired via

electronic hardware and analyzed using a computer (**Figure** 3a) (Experimental Section, *Electrical measurement*). To determine the capture location for each cell processed on the device, we processed the output signal using a custom-built decoding algorithm (**Figure** 3b). The algorithm was implemented in the LabVIEW (National Instruments) and processed the data with minimal manual intervention.[30] Briefly, our algorithm first reviewed a part of the recorded electrical waveform, identified different code signals present, and classified them into different sensor groups. Once each sensor group contains a sufficient number of code signal instances, signals were normalized and averaged to form a library of code templates that correspond to each and every sensor in the network. The generation of templates based on recorded signals from the sample itself made the templates specific to both the sample and the device, thereby increasing accuracy. The templates were then used to process all sensor data by correlating the output signal with the template library. Because the code signals were specifically designed to be mutually orthogonal, we could not only classify sensor signals robustly with minimal crosstalk but also resolve signal interferences through an iterative process called successive interference cancellation.[30,35] At the end of this decoding process, the original output waveform was decomposed into data from individual sensors, which was then used to calculate cell capture statistics across the whole device. Specifically, the number of captured cells in each chamber was obtained, by subtracting the exit node cell count from the entry node cell count. (**Table** 1.1 and 1.2).

### 2.2. Optimization of the cell capture parameters

Cells expressing the target antigens and yet not captured by our device lead to false negative results. Therefore, to maximize cell capture efficiency, we first optimized the amount of antibody to coat the microfluidic cell capture chambers. To measure the antibody coverage on the surface, we employed fluorophore-conjugated antibodies and imaged the functionalized

device with fluorescence microscopy. Cell capture chambers were first functionalized with FITC anti-CD45 antibody at concentrations ranging from 0.25 μg $mL^{-1}$ to 50 μg $mL^{-1}$ using the immobilization protocol (Experimental Section, *Immobilization of antibodies in the microfluidic device*). We observed higher fluorescence emission with increasing antibody concentration, and the differential emission between antibody concentrations was especially apparent on micropillar surfaces, where deposited fluorophore-conjugated antibody formed high contrast annular patterns around the cross-sections of the pillars (**Figure** 4a). Quantitative measurements of mean fluorescence intensities for different concentrations showed a drastic increase in surface antibody concentration until 10 μg $mL^{-1}$ and the changes in fluorescence beyond 25 μg $mL^{-1}$ were not notable, indicating surface saturation (**Figure** 4a). Based on these results, we selected 25 μg $mL^{-1}$ as the optimum incubation concentration to ensure complete coverage of the device surface with capture antibodies.

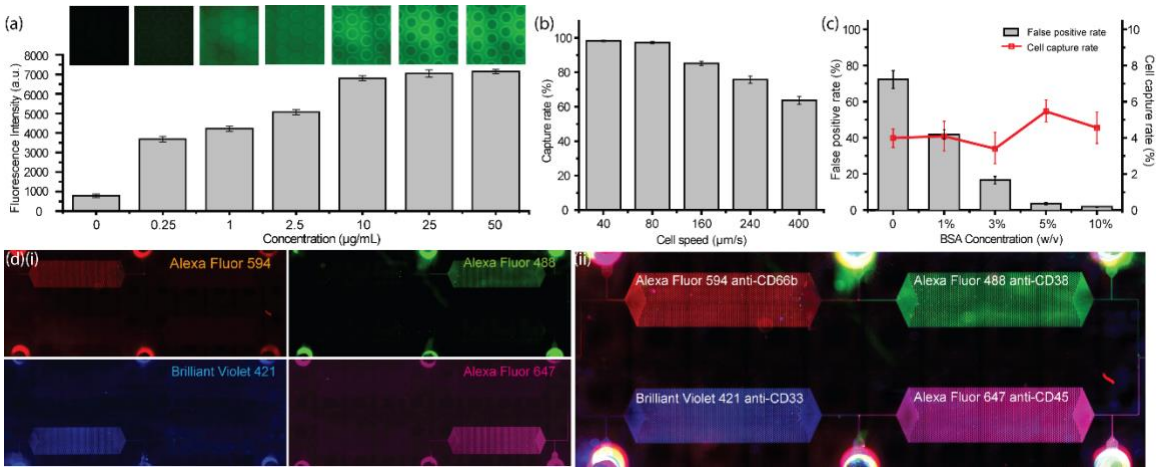


**Figure 4.** Optimization of the surface chemistry and processing conditions for efficient cell capture in microfluidic chambers. (a) Optimization of the capture antibody amount immobilized on the device surface. Devices were functionalized with FITC-conjugated anti-CD45 antibody at concentrations ranging from 0 to 50 μg $mL^{-1}$. The amount of the immobilized antibody at different concentrations was measured from the fluorescence intensity. (b) Optimization of the sample flow speed. Measured leukocyte capture rates in devices functionalized with anti-CD45 as a function of sample flow rates ranging from 40 μm $s^{-1}$ to 400 μm $s^{-1}$. (c) Optimization of the BSA concentration for minimizing non-specific cell capture. Non-specific cell capture rate was measured at BSA concentrations ranging from 0 to

10%. (d) Specific functionalization of microfluidic chambers with four different capture antibodies. (i) Single-channel fluorescence images show the exclusive immobilization of capture antibodies, each labeled with a different fluorophore, in the corresponding cell capture chambers. Each capture chamber is uniformly coated, and no crosstalk can be observed between cell capture chambers. (ii) A four-channel fluorescence image of the whole device shows the successful functionalization of cell capture chambers. The boundaries between different antibodies are visible along the microfluidic channels that connect cell capture chambers. (Error bars represent standard deviation.)

We also investigated the sample flow speed as a parameter to optimize the cell capture rate in our microfluidic device. The flow speed is an important factor in our assay because the cell immunocapture is a process with a binary outcome that depends on both the number of matching antibody-antigen pairs and the antibody-antigen interaction time, controlled by the sample flow speed.[36,37] To optimize sample flow speed, we first functionalized the cell capture chambers with anti-CD45 antibody and tested the leukocyte capture performance under different flow rates. To quantify the effect of sample flow speed on the capture rate, we drove leukocytes through the microfluidic device at flow speeds ranging from 40 μm $s^{-1}$ to 400 μm $s^{-1}$ using a syringe pump and measured the fraction of captured cells in the microfluidic chamber. As anticipated, the cell capture rate showed a strong dependence on the flow speed decreasing from ~99% for flow rates 80 μm $s^{-1}$ to ~64% at 400 μm $s^{-1}$ (**Figure** 4b). Based on minimal observed differences between cell capture rates below 80 μm $s^{-1}$ and considering potential problems at low flow rates such as sedimentation and non-specific adhesion induced artifacts, we chose 80 μm $s^{-1}$ as the optimal sample flow speed for our assay. Similar optimization experiments have also been performed for the other antibodies used in this work, and we found that at 80 μm $s^{-1}$, all produced >96% capture rates. It should also be noted that the sample flow speed could be used as a physical gating mechanism since the required number of the antibody-antigen pairs in the cell adhesion process is related to the interface contact time.[37] For example, a higher cell velocity would increase the minimum number of the antibody-antigen pairs required for cell capture, which would be analogous to a

lower gate size in the post-analysis of flow cytometry data. Likewise, a lower flow velocity can be used to compensate for a low affinity antibody-antigen pair and enhance the assay sensitivity.

To ensure specific capture of target cells in microfluidic capture chambers, we minimized non-specific cell adhesion by blocking the functionalized device surface with bovine serum albumin (BSA). To determine the optimum BSA amount, we first functionalized devices at the predetermined optimum antibody concentration (25 μg $mL^{-1}$) and treated them with BSA solutions with concentrations ranging from 0 to 10% (w/v) for 1 hour. After washing the devices with PBS, we drove leukocytes at the optimum flow speed (80 μm $s^{-1}$) and measured the non-specific cell capture rate. In these measurements, we specifically chose the anti-CD115 as the capture antibody since the CD115 is expressed only by <10% of leukocytes (i.e., some monocytes),[38] making most leukocytes potential targets for the non-specific capture. To distinguish specific monocyte capture from non-specific cell capture, captured leukocytes were post-labeled with Alexa Fluor 488 anti-CD115 and counted with fluorescence microscopy. With increasing BSA concentration, non-specific cell capture rate decreased from >70% for non-blocked devices to ~2% for devices treated with a 10% BSA solution (**Figure** 4c). Finally, we confirmed that specific cell capture was not confounded by blocking, because the capture rate of $CD115^{pos}$ leukocytes remained virtually constant across different BSA concentrations (**Figure** 4c, red line). Based on these results, we selected the 10% BSA solution as the optimal blocking buffer for our assay.

Following the optimization of surface chemistry for efficient and specific cell capture, we investigated the selective immobilization of capture antibodies to designated cell capture chambers. Specifically, we attempted to coat each of the four cell capture chambers with a

different antibody via auxiliary functionalization ports based on the protocol described previously and inspected the resultant spatial arrangement of antibodies across the device with microscopy. To distinguish between different antibodies on the device, we specifically used antibodies conjugated with different-colored fluorophores (Alexa Fluor 594, Alexa Fluor 488, Brilliant Violet 421, and Alexa Fluor 647). Fluorescence images of the functionalized device showed that (1) each cell capture chamber was exclusively coated with the intended capture antibody (**Figure** 4d(i)), (2) there was no crosstalk between the different chambers as evidenced by distinct boundaries between different immobilized antibodies in the microfluidic channels that connect cell capture chambers (**Figure** 4d(ii)), and (3) the antibody coverage was uniform throughout all cell capture chambers. It should also be noted that antibodies immobilized external to the cell capture chambers do not constitute a problem for our assay since (1) cells flow much faster (40 ×) in microfluidic channels preventing them to be captured on electrodes and (2) any cell trapped at the inlet or outlet reservoirs due to slower flow remain outside of the electrical detection nodes and therefore are not counted.

### 2.3. Immunophenotyping of tumor cell mixtures

For controlled experiments to validate our assay, we employed human cancer cell lines with differing antigen expression. We cultured three breast cancer cell lines (MCF7, SK-BR-3, and MDA-MB-231) and selectively functionalized cell capture chambers with two different antibodies (anti-EpCAM and anti-CD49f antibodies) specifically chosen to target antigens that are differentially expressed by those breast cancer cell lines: MCF7: $EpCAM^{pos}CD49f^{neg}$, SK-BR-3: $EpCAM^{pos}CD49f^{pos}$, MDA-MB-231: $EpCAM^{low/neg}CD49f^{pos}$ with a secondary $EpCAM^{low/neg}CD49f^{neg}$ immunophenotype.[39] To distinguish these immunophenotypes, we arranged the anti-EpCAM and anti-CD49f antibodies in cell capture chambers as a 2 × 2 checkerboard pattern (**Figure** 5a), which enabled us to screen cells for all possible

combinations of EpCAM and CD49f expressions. Based on the individual cell counts from the coded electrical sensors on the microfluidic device (**Table** 1.1), we were able to calculate the fraction of cells captured in each cell capture chamber (**Table** 1.2) and use the measured cell capture statistics to calculate the prevalence of each combinatorial immunophenotype (**Table** 1.3) in the sample.

**Table 1.1.** The Gold codes used in the multiplexed sensor network for the antibody microarray and the individual cell count from each coded Coulter sensor

| Coded sensor | Code | Cell count |
|---|---|---|
| Code 1,1 | 10101110110001111100110100100000 | $c_{11}$ |
| Code 1,2 | 00011011110110100011111110100000 | $c_{12}$ |
| Code 1,3 | 01110010110100001101001100111110 | $c_{13}$ |
| Code 2,1 | 10110101000111011111001001100000 | $c_{21}$ |
| Code 2,2 | 01001100101110011101100111010000 | $c_{22}$ |
| Code 2,3 | 10010100010000000111110111111101 | $c_{23}$ |

**Table 1.2.** The calculation of the fraction of cells captured in each chamber and non-captured cells discharged into the waste from electrical data

| Chamber | Immunophenotype | Fraction |
|---|---|---|
| Chamber 1,1 | $EpCAM^{pos}$ | $p_{11}=(c_{11}-c_{12})/c_{11}$ |
| Chamber 1,2 | $EpCAM^{neg}CD49f^{pos}$ | $p_{12}=(c_{12}-c_{13})/c_{11}$ |
| Outlet 1 | $EpCAM^{neg}CD49f^{neg}$ | $p_{1end}=c_{13}/c_{11}$ |
| Chamber 2,1 | $CD49f^{pos}$ | $p_{21}=(c_{21}-c_{22})/c_{21}$ |
| Chamber 2,2 | $CD49f^{neg}EpCAM^{pos}$ | $p_{22}=(c_{22}-c_{23})/c_{21}$ |
| Outlet 2 | $CD49f^{neg}EpCAM^{neg}$ | $p_{2end}=c_{23}/c_{21}$ |

**Table 1.3.** The calculation of the target subpopulation fractions in the cell mixture from the electrical data

| Combinatorial immunophenotype | Fraction |
|---|---|
| $EpCAM^{pos}CD49f^{pos}$ | $1-p_{12}-p_{22}-(p_{1end}+p_{2end})/2$ |
| $EpCAM^{pos}CD49f^{neg}$ | $p_{22}$ |
| $EpCAM^{neg}CD49f^{pos}$ | $p_{12}$ |
| $EpCAM^{neg}CD49f^{neg}$ | $(p_{1end}+p_{2end})/2$ |

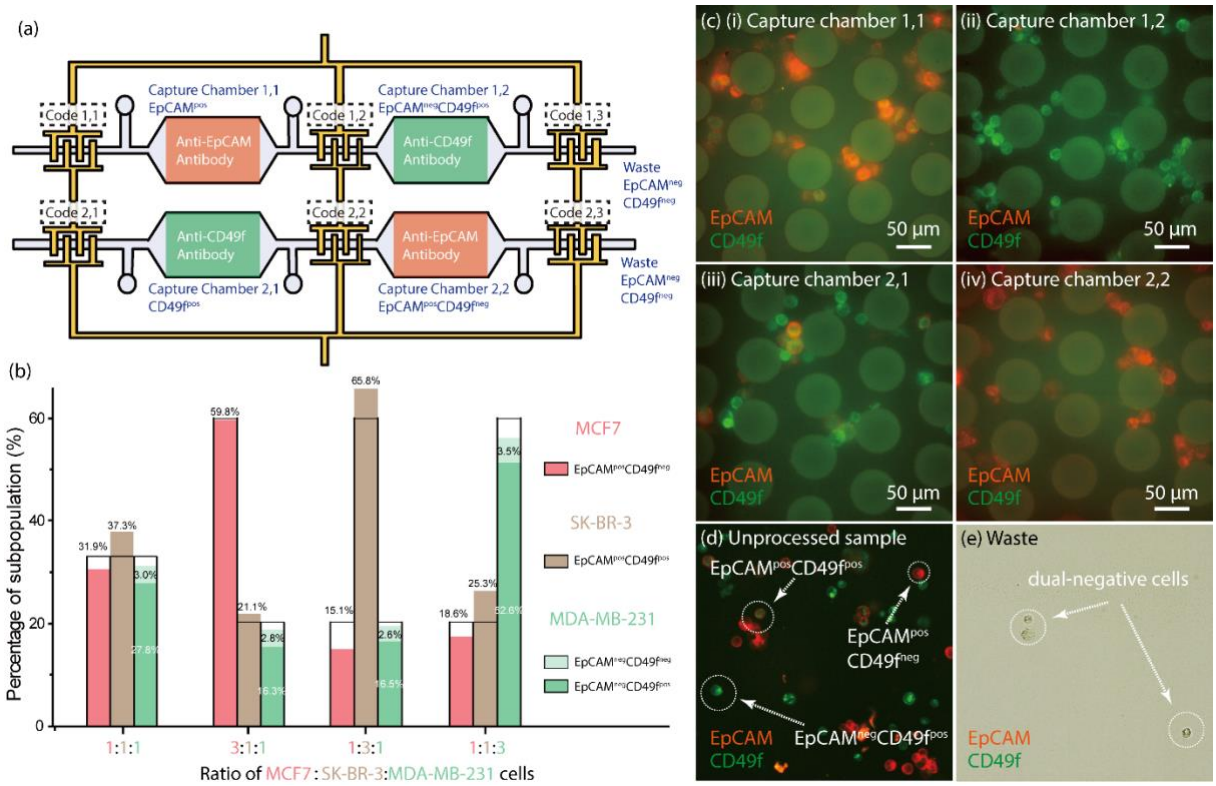


**Figure 5.** Immunophenotyping of tumor cell mixtures. (a) A schematic showing the specific antibody arrangement in the designed microarray. Anti-EpCAM and anti-CD49f antibodies are immobilized in chambers with a checkerboard pattern to fractionate mixtures of MCF7 ($EpCAM^{pos}CD49f^{neg}$), SK-BR-3 ($EpCAM^{pos}CD49f^{pos}$), and MDA-MB-231 ($EpCAM^{low/neg}CD49f^{pos}$) and dual-negative ($EpCAM^{neg}CD49f^{neg}$) cells, which are discharged from the waste outlet. (b) Comparison of the measured frequency (colored bar) and the mix ratios (overlaid unshaded bar) of different cancer cell lines in control samples. Four control samples were prepared by mixing MCF7, SK-BR-3, and MDA-MB-231 cancer cell lines at ratios of 1:1:1, 3:1:1, 1:3:1, and 1:1:3. (c) Representative two-channel fluorescence images of the captured cells post-labeled with a cocktail of Alexa Fluor 594 anti-EpCAM and Alexa Fluor 488 anti-CD49f antibodies in (i) chamber 1,1 ($EpCAM^{pos}$), (ii) chamber 1,2 ($EpCAM^{neg}CD49f^{pos}$), (iii) chamber 2,1 ($CD49f^{pos}$), and (iv) chamber 2,2 ($CD49f^{neg}EpCAM^{pos}$). (d) The fluorescence image of the unprocessed sample stained with the same fluorophore-conjugated antibodies show all combinatorial immunophenotypes ($EpCAM^{pos}CD49f^{pos}$, $EpCAM^{pos}CD49f^{neg}$, and $EpCAM^{low/neg}CD49f^{pos}$). (e) A fluorescence image of cells ($EpCAM^{neg}CD49f^{neg}$) found in the waste collected from our device. Post-labeling of cells against the two antibodies produced no fluorescence signal indicating the dual-negative immunophenotype of these cells.

To test our assay's performance in identifying subpopulations with different antigen expressions, we processed suspensions of MCF7, SK-BR-3, and MDA-MB-231 cancer cells mixed at varying ratios as heterogenous control samples at a flow rate of 80 µm $s^{-1}$. Our electronic results on the immunophenotype composition of different cell mixtures were

consistently in good agreement with the designed mix ratios (**Figure** 5b). The differences were mainly due to co-expression of the same immunophenotype by two different cancer cell lines, e.g., MDA-MB-231 cells also express EpCAM, at a low concentration, and were counted in the $EpCAM^{pos}CD49f^{pos}$ immunophenotype that was interpreted as SK-BR-3. Nevertheless, this is not a fundamental problem as measurements can be computationally corrected to accommodate crosstalk between immunophenotypes based on projected antigen co-expression rates of target cell subtypes in a given population.

To independently validate cell immunophenotype discrimination by our assay, we characterized the expression of tumor cells captured on the chip via fluorescence microscopy after post-labeling them against both EpCAM and CD49f. From the dual-channel fluorescence images of stained cells, differences in the composition of cells captured in different chambers could clearly be observed: Anterior cell capture chambers in the microfluidic cascade (i.e., chambers 1,1 and 2,1) received the full sample composition and captured cells that expressed the target antigen (i.e., EpCAM for chamber 1,1 (**Figure** 5c(i)) and CD49f for chamber 2,1 (**Figure** 5c(iii))). In both anterior cell capture chambers, dual-expressor cells could also be observed as the expression of another antigen did not interfere with the cell immunocapture. In contrast, cells captured in posterior chambers contained only single-expressor cells with the antigen targeted by the capture antibody immobilized in the corresponding capture chamber (CD49f for chamber 1,2 (**Figure** 5c(ii)) and EpCAM for chamber 2,2 (**Figure** 5c(iv))). The lack of dual-expressor cells in the posterior chambers is due to the fact that posterior cell capture chambers received only a portion of the sample that was already depleted of cells expressing the antigen targeted by the anterior chamber. As a control, we labeled cells in the unprocessed (input) mixture and also in the waste (output) with the same fluorophore-conjugated antibodies and observed cells in the unprocessed

sample expressed all possible immunophenotypes (**Figure** 5d), while cells in the waste were all dual-negative expressing neither EpCAM nor CD49f (**Figure** 5e). Taken together, these results demonstrated a successful fractionation of a heterogeneous sample into different cell capture chambers based on the cell immunophenotype and validated the platform for combinatorial phenotyping of cell populations.

### 2.4. Immunophenotyping of leukocytes

To demonstrate the relevance of our assay for point-of-care testing, we designed an assay to measure the composition of leukocytes in a blood sample. To distinguish different leukocyte subpopulations, we functionalized our device with four different antibodies (anti-CD66b, anti-CD38, anti-CD33, anti-CD45) against antigens differentially expressed among leukocytes. Importantly, the spatial arrangement of antibodies on the device (**Figure** 6a) were specifically designed to distinguish different leukocyte subtypes with distinct immunophenotypes, namely granulocytes, lymphocytes, and monocytes: In one of the microfluidic paths, antibodies were immobilized in a sequence, where the anti-CD66 was followed by the anti-CD38. Under this arrangement, cells captured in the anterior chamber (i.e., $CD66b^{pos}$ immunophenotype) were considered as granulocytes,[40] while cells in the posterior chamber (i.e., $CD66b^{neg}CD38^{pos}$ immunophenotype) were considered as lymphocytes.[41,42] In the other microfluidic path, the anti-CD33 was followed by the anti-CD45. Because CD33 is a surface marker used for identifying monocytes, that is also expressed by granulocytes,[43,44] we interpreted cells captured in the anterior chamber (i.e., $CD33^{pos}$ immunophenotype) as a mixed population of monocytes and granulocytes, while cells in the posterior chamber (i.e., $CD33^{neg}CD45^{pos}$ immunophenotype) were considered as granulocytes and lymphocytes. By processing electrical sensor data, we could determine the capture statistics for each immunophenotype

(**Table** 2.1) and calculate the frequency of each leukocyte subpopulation (**Table** 2.2) in the blood sample.

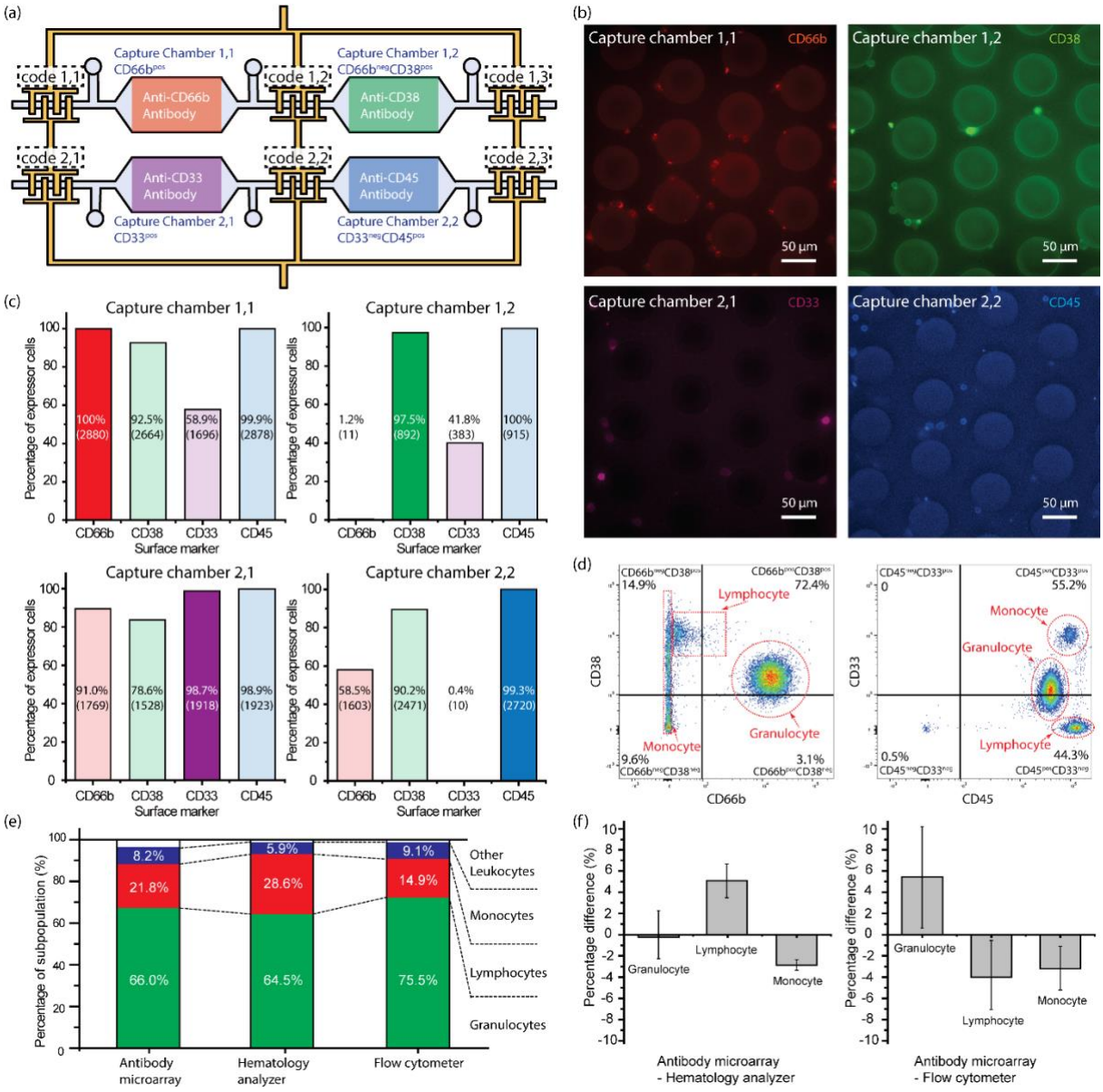


**Figure 6.** Immunophenotyping of leukocytes. (a) A schematic showing the specific antibody arrangement in the microarray. Microfluidic cell capture chambers were functionalized with anti-CD66b, anti-CD38, anti-CD33, and anti-CD45 antibodies to fractionate leukocytes into granulocytes, lymphocytes, and monocytes. (b) The single-channel fluorescent images showing surface marker expressions on the captured cells in different microfluidic chambers. The images show all captured cells expressing the antigen targeted by the corresponding capture chamber. (c) Immuno-expression of cells captured in each microfluidic chamber. All of the captured cells were labeled with fluorophore-conjugated antibodies against all four antigens, and the frequency of each immunophenotype was calculated for each cell capture chamber. Each bar in the plots shows the measured frequency and the actual cell count for the

immunophenotype in the corresponding capture chamber. (d) Classification of leukocyte subpopulations with flow cytometry. The density scatter plots show frequencies of the subpopulations for each immunophenotype. The gates in the plots were set based on the prior tests with fluorophore-labeled calibration beads. The measurements were grouped as granulocyte, lymphocyte, or monocyte based on the cell hierarchy population analysis from the FSC-SSC plot (**Figure** S2) for better illustration. (e) The frequency of leukocyte subpopulations measured by our device, a commercial hematology analyzer, and a commercial flow cytometer in matched samples. (f) The average difference in the measurement of leukocyte subpopulations using our device versus the hematology analyzer (left), and the flow cytometer (right). Error bars represent standard deviation.

**Table 2.1.** The immunophenotype, calculation of the fractions, and the types of cells captured in each chamber and non-captured cells discharged into the waste

| Chamber | Immunophenotype | Fraction | Cell type |
|---|---|---|---|
| Chamber 1,1 | $CD66b^{pos}$ | $p_{11}=(c_{11}-c_{12})/c_{11}$ | Granulocytes |
| Chamber 1,2 | $CD66b^{neg}CD38^{pos}$ | $p_{12}=(c_{12}-c_{13})/c_{11}$ | Lymphocytes |
| Outlet 1 | $CD66b^{neg}CD38^{neg}$ | $p_{1end}=c_{13}/c_{11}$ | |
| Chamber 2,1 | $CD33^{pos}$ | $p_{21}=(c_{21}-c_{22})/c_{21}$ | Monocytes + Granulocytes |
| Chamber 2,2 | $CD33^{neg}CD45^{pos}$ | $p_{22}=(c_{22}-c_{23})/c_{21}$ | Lymphocytes + Granulocytes |
| Outlet 2 | $CD33^{neg}CD45^{neg}$ | $p_{2end}=c_{23}/c_{21}$ | Other leukocytes |

**Table 2.2.** The parametric calculation of the fraction of each leukocyte subtype in the leukocyte suspension

| Leukocyte Subtype | Fraction |
|---|---|
| Granulocytes | $p_{11}$ |
| Lymphocytes | $p_{12}$ |
| Monocytes | $1-p_{11}-p_{12}-p_{2end}$ |

We applied our technology on blood samples collected from consenting donors and validated our results by fluorescently labeling and imaging of leukocytes captured on our device. Following the lysis of erythrocytes, >4000 leukocytes were processed using our assay in 10-15 minutes at a flow rate of 80 μm $s^{-1}$. Following the completion of the assay, cells were immunolabeled on the chip with a cocktail of Alexa Fluor 594 anti-CD66b, Alexa Fluor 488 anti-CD38, Alexa Fluor 647 anti-CD33, and Brilliant Violet 421 anti-CD45 antibodies and characterized with a fluorescence microscope. Fluorescence measurements confirmed that virtually all captured leukocytes expressed the surface antigen targeted by the corresponding capture chamber (**Figure** 6b). By imaging all leukocytes on the chip in different fluorescence channels (**Figure** S1), we measured the frequency of expression for all four antigens in each

capture chamber (**Figure** 6c). This complete picture of cell composition demonstrated that (1) our microfluidic device was very efficient in capturing target cells, (2) cell population captured in different chambers showed drastic differences in their expression profile, further confirming successful sample fractionation into distinct subpopulations.

To assess the performance of our technique for blood analysis, we benchmarked our results against measurements from established hematology techniques. Matching blood samples were processed with a commercial benchtop hematology analyzer (CELL-DYN Ruby, Abbott) to obtain a complete blood count and also with a flow cytometer (BD LSRFortessa). For the flow cytometry, the leukocyte suspension was fluorescently labeled against the same set of antigens employed in our assay, and the results were gated based on preconfigured values for leukocyte classification to calculate the frequency of each subpopulation (**Figure** 6d and S2). Considering the differences between the complete blood count and flow cytometry results, our results are in agreement with both techniques (**Figure** 6e); the percentage of $CD66b^{pos}$ cells (granulocytes) measured by our device, hematology analyzer, and flow cytometer were 66.0%, 64.5%, and 75.5%, respectively; the percentage of $CD66b^{neg}CD38^{pos}$ cells (monocytes) was measured as 21.8% with the antibody microarray, 28.6% with the hematology analyzer, and 14.9% with the flow cytometer; the frequency of the $CD33^{pos}$ cells was determined by our device to be 43.0% versus 55.2% from the flow cytometer. Our repeated measurements on blood samples collected from different donors showed that our device could accurately identify leukocyte subpopulations with an average of <6% difference from complete blood count and flow cytometry results (**Figure** 6f). Observed differences between these measurements should be expected due to several factors: (1) transduction modalities of the three methods are fundamentally different, leading to entirely different discrimination criteria to classify different subpopulations, (2) artifacts are unavoidably

introduced during different sample preparation steps required for different techniques, e.g., erythrocyte residues in the lysed samples or cell loss during centrifugation processes.

The electronic antibody microarray, introduced in this work, is a viable immunophenotyping assay with several advantages over existing methods for the analysis of cell populations. First, our technique is label-free. In a typical flow cytometry assay, the samples have to be pre-labeled with fluorophore-conjugated antibodies to transduce chemical information into optical signals,[16,45] while unlabeled cells can directly be introduced into our assay for analysis. The label-free operation not only makes our approach well suited for settings where sample preparation is not feasible but also reduces the total assay time, thereby increasing its practical utility. Second, our assay directly reports immunophenotyping results as electrical data. Compared to optical systems, which require both optical and electrical components, our platform can be coupled with an electronic circuit that can both drive and read the on-chip sensors, reducing both the system complexity and size. Compared to conventional electrical cytometry that measures physical properties of cells (e.g., size[46] and electrical parameters[47]), our technique probes well-established and more specific biochemical markers on the cell membrane, which cannot be probed through electrical means otherwise. On-chip multiplexing of electrical data enables an efficient acquisition, storage, transmission, and analysis of the assay results. In fact, computational analysis of the assay results could be performed in real-time (~1000 cells $s^{-1}$) using deep learning algorithms.[48] Overall, our platform operates as simple as a Coulter counter supported with more advanced software to interpret its results. Third, our assay is both flexible and scalable to screen for a specific and larger number of antigen combinations, respectively. Flow cytometers are limited in the number of antigens that can be probed simultaneously due to spectral crosstalk in the detectors.[16,45] In contrast, our platform can add more capture chambers and sensors without

affecting the performance of existing sensors.[35] Compared to conventional antibody microarrays,[49,50] on the other hand, our assay can identify subpopulations expressing different antigen combinations by sequentially subjecting the cells to different antibodies. Taken together, label-free immunophenotyping of cell populations against multiple targets on an electronic disposable chip presents an opportunity in global health and telemedicine applications for cell-based diagnostics and health monitoring.

## 3. Conclusion

We introduced a microfluidic antibody microarray that can electrically report the frequency of target cell subpopulations in a sample. In our device, functionalized microfluidic chambers cascaded to produce different antibody combinations fractionate samples into its components, and an integrated sensor network transduces cell capture statistics into electrical data for label-free immunophenotyping. Remarkably, the application of our technique for the analysis of leukocyte subpopulations in blood samples produced comparable results with significantly more expensive and sophisticated commercial systems, both validating the assay accuracy and demonstrating its potential utility. All in all, we believe the ability to electrically screen cell immunophenotypes on a disposable chip that can be scaled and tuned for specific cell subsets could be transformative in cell-based diagnostics at the point-of-care and resource-limited scenarios.

## 4. Experimental Section

*Chemicals and materials*: Ammonium chloride ($NH_4Cl$), potassium bicarbonate ($KHCO_3$), ethylenediaminetetraacetic acid (EDTA) tetrasodium salt, glutaraldehyde, and trichloro(octyl)silane were purchased from Sigma-Aldrich (St. Louis, MO), pure ethanol were purchased from Decon Labs, Inc. (Kings of Prussia, PA), APTES was purchased from Gelest,

Inc. (Morrisville, PA), BSA was purchased from Thermo Scientific (Rockford, IL), 1× PBS was purchased from Mediatech (Manassas, VA), all chemicals are analytical grade. All water used for the experiment was deionized (DI) water.

Alexa Fluor 594 anti-CD66b antibody (G10F5 clone), Alexa Fluor 488 anti-CD38 antibody (HIT2 clone), Brilliant Violet 421 anti-CD33 antibody (WM53 clone), Alexa Fluor 647 anti-CD45 antibody (2D1 clone), FITC anti-CD45 antibody (2D1 clone), anti-CD45 antibody (2D1 clone), anti-CD115 antibody (9-4D2-1E4 clone), Alexa Fluor 488 anti-CD115 antibody (9-4D2-1E4 clone), anti-EpCAM antibody (9C4 clone), anti-CD49f antibody (GoH3 clone), Alexa Fluor 594 anti-EpCAM antibody (9C4 clone), Alexa Fluor 488 anti-CD49f antibody (GoH3 clone), anti-CD66b antibody (G10F5 clone), anti-CD38 antibody (HIT2 clone), anti-CD33 antibody (WM53 clone), Alexa Fluor 647 anti-CD33 antibody (WM53 clone), Brilliant Violet 421 anti-CD45 antibody (2D1 clone), PE anti-CD66b antibody (G10F5 clone), APC anti-CD38 antibody (HIT2 clone), PE anti-CD45 antibody (2D1 clone), and APC anti-CD33 (WM53 clone) antibody were all purchased from Biolegend (San Diego, CA).

4-inch silicon wafers were purchased from UniversityWafer, Inc. (South Boston, MA), SU-8 2000 series photoresist was purchased from MicroChem (Westborough, MA), NR9-1500PY negative photoresist was purchased from Futurrex, Inc. (Franklin, NJ), PDMS elastomer Sylgard 184 was purchased from Dow Corning (Auburn, MI).

MCF7 (ATCC® HTB-22™), SK-BR-3 (ATCC® HTB-30™), and MDA-MB-231 (ATCC® HTB-26™) breast cancer cell lines were obtained from American Type Culture Collection (ATCC) (Manassas, VA), Dulbecco's Modified Eagle's Medium (DMEM) medium was purchased from Mediatech (Manassas, VA), fetal bovine serum (FBS) was purchased from

Seradigm (Radnor, PA), 0.25% trypsin-EDTA was purchased from Life Technologies (Carlsbad, CA).

The blood samples were obtained via venipuncture from healthy donors' bodies using an informed consent process according to the Georgia Tech IRB protocol approved by Georgia Tech IRB.

*Fabrication of the microfluidic device*: We fabricated our device using a combination of soft lithography and surface micromachining. The PDMS microfluidic layer was fabricated using soft lithography. To fabricate the mold, we coated a 4-inch silicon wafer with a SU-8 negative photoresist film and patterned the photoresist with photolithography. The mold was then treated with trichloro(octyl)silane for 6 hours to increase the surface hydrophobicity for the demolding process. PDMS prepolymer and crosslinker were mixed at a 10:1 ratio, poured on the mold, degassed in vacuum, and cured for 4 hours in an oven at 65 °C. The cured PDMS was then peeled off from the mold, and fluidic inlet, outlet, and auxiliary functionalization ports were created with a biopsy punch. Separately, the electrical sensor network was fabricated using a lift-off process. For the sensor fabrication, a 1.2 μm-thick NR9 negative photoresist was spun on a 3 by 2-inch glass slide, patterned using a maskless aligner (MLA150, Heidelberg), followed by the evaporation of a 20 nm/480 nm Cr/Au film stack. The sacrificial photoresist was etched in an acetone bath. The PDMS layer and the glass substrate were then surface activated in an oxygen plasma environment, aligned under a microscope, and permanently bonded together to form the final device (**Figure** 1b).

*Immobilization of antibodies in the microfluidic device***:** We employed a four-step chemical modification protocol at room temperature to functionalize the cell capture chambers with

antibodies (**Figure** S3). First, the microfluidic device was wetted with ethanol, and within 10 minutes of the PDMS-glass bonding, APTES in ethanol (2% v/v) was introduced to the device and incubated for 30 minutes. Second, the device was rinsed with ethanol and DI water and a glutaraldehyde solution in DI water (1% v/v) was introduced and incubated for 30 minutes. Third, the device was rinsed with DI water and PBS, and capture antibodies in PBS were introduced into the cell capture chambers and incubated for 1 hour. Fourth, the device was washed with PBS to remove unbound antibodies, and the cell capture chambers were incubated with BSA blocking buffer for 1 hour to block the non-specific binding sites. Finally, the device was rinsed with PBS to complete the functionalization process.

*Human cancer cell line culture*: We prepared mixtures of human cancer cell lines with different surface antigen expression as control samples to characterize the performance of our device. Three different breast cancer cell lines, MCF7, SK-BR-3, and MDA-MB-231 were cultured in DMEM media supplemented with 10% FBS and maintained under 5% $CO_2$ atmosphere at 37 °C in an incubator. Once 80% confluence reached, cells were detached in a 0.25% trypsin solution, pelleted in a centrifuge, resuspended in 1× PBS, and mixed by gentle pipetting to mechanically dissociate potential cell aggregates. Cell concentration for each cell type was measured with a microscope and different cell lines were mixed at known ratios to create control samples with heterogeneous cell populations.

*Human blood sample processing*: 1 mL blood samples were collected from healthy donors according to an IRB-approved protocol. To ensure against coagulation, all blood samples were collected in BD EDTA tubes, stored on a rocker at room temperature, and were processed within 6 hours of the blood withdrawal. Prior to processing on our assay, we lysed erythrocytes, which greatly outnumber leukocytes. For our assay, erythrocytes would not only

hinder contact between the leukocytes and the functionalized device surface,[51] but also increase the background noise in electrical signals and decrease the SNR in electrical measurements. To lyse erythrocytes, we treated the blood sample with ammonium-chloride-potassium (ACK) buffer for ~15 minutes and subsequently centrifuged at 350 xg for 5 minutes. The supernatant was removed, and the cell pellet was rinsed twice with PBS to remove erythrocyte residues. The cell pellet was then suspended in PBS with gentle pipetting, filtered using 35 μm nylon mesh incorporated Cell Strainer Snap Cap (Falcon, Corning) to create the leukocyte suspension for our assay.

*Electrical measurement*: We measured cell capture rates for all microfluidic chambers by electrically tracking cell flow on the assay with the integrated electrical sensor network. To detect coded impedance modulations from cells flowing across the microfluidic assay, the device was excited from the common electrode terminal with a 1 V sine wave at 500 kHz supplied from the output of the lock-in amplifier (HF2LI, Zurich Instruments), and the resulting current signals were acquired from the two sensing electrodes. The current signals were first converted into voltage signals using two transimpedance amplifiers, and then subtracted from each other with a differential amplifier to produce a single electrical waveform. The amplitude of the electrical signal was measured with the lock-in amplifier, and sampled to a computer for digital signal processing.

**Supporting Information**
Supporting Information is available from the Wiley Online Library or from the author.

**Acknowledgements**
This work was supported by the Arnold and Mabel Beckman Foundation, USA (Beckman Young Investigator Award to A.F.S.) and the National Science Foundation, USA (Award no. ECCS 1752170). The authors would like to thank Dr. Minati Satpathy for her helpful discussions on the selection of cancer cell lines as control samples. The authors would also like to acknowledge Prof. Vladimir Tsukruk, Prof. Loren Williams, and Dr. Nidhi Williams of

the Georgia Institute of Technology for their helpful suggestions on surface modification procedures. The authors would like to thank all healthy volunteers who contributed blood samples for this study.

Received: ((will be filled in by the editorial staff))
Revised: ((will be filled in by the editorial staff))
Published online: ((will be filled in by the editorial staff))

## References

[1] H. Zola, *Mol. Med.*, **2006**, *12*, 312.

[2] E. Dabelsteen, U. Mandel, H. C. Clausen, *Crit. Rev. Oral Biol. Med.*, **1991**, *2*, 493.

[3] L. Belov, O. de la Vega, C. G. dos Remedios, S. P. Mulligan, R. I. Christopherson, *Cancer Res.*, **2001**, *61*, 4483.

[4] Human Cell Differentiation Molecules (HCDM), http://www.hcdm.org/, August 2019.

[5] S. R. Bennett, F. R. Carbone, F. Karamalis, R. A. Flavell, J. F. A. P. Miller, W. R. Heath, *Nature*, **1998**, *393*, 478.

[6] N. Baumgrath, In: *Methods in Cell Biology* Vol. 75 (Eds: Z. Darzynkiewicz, M. Roederer, H. Tanke). Elsevier, New York, NY, USA **2004**, 643.

[7] J. S. Han, P. P. Nair, *Cancer*, **1995**, *76*, 195.

[8] A. Adan, G. Alizada, Y. Kiraz, Y. Baran, A. Nalbant, *Crit. Rev. Biotechnol.*, **2017**, *37*, 163.

[9] E. Coustan-Smith, J. Sancho, F. G. Behm, M. L. Hancock, B. I. Eazzouk, R. C. Ribeiro, G. K. Rivera, J. E. Rubnitz, J. T. Sandlund, C. H. Pui, D. Campana, *Blood*, **2002**, *100*, 52.

[10] C. Riccardi, I. Nicoletti, *Nat. Protoc.*, **2006**, *1*, 1458.

[11] M. A. Van Dilla, R. G. Langlois, D. Pinkel, D. Yajko, W. K. Hadley, *Science*, **1983**, *220*, 620.

[12] T. Inoue, A. Swain, Y. Nakanishi, D. Sugiyama, *Anticancer Res.*, **2014**, *34*, 4539.

[13] O. Civelekoglu, N. Wang, M. Boya, T. Ozkaya-Ahmadov, R. Liu, A. F. Sarioglu, *Lab*

*Chip*, **2019**, *19*, 2444.

[14] S. C. De Rosa, L. A. Herzenberg, L. A. Herzenberg, M. Roederer, *Nat. Med.*, **2001**, *7*, 245.

[15] M. Al-Hajj, M. S. Wicha, A. Benito-Hernandez, S. J. Morrison, M. F. Clarke, *Proc. Natl. Acad. Sci. U. S. A.*, **2003**, *100*, 3983.

[16] Y. Saeys, S. Van Gassen, B. N. Lambreche, *Nat. Rev. Immunol.*, **2016**, *16*, 449.

[17] W. Li, Y. Gao, D. Pappas, *Biomed Microdevices*, **2015**, *17*, 113.

[18] Y. Zhang, Y. Zhou, W. Li, V. Lyons, A. Johnson, A. Venable, J. Griswold, D. Pappas, *Anal. Chem.*, **2018**, *90*, 7204.

[19] M. A. Qasaimeh, Y. C. Wu, S. Bose, A. Menachery, S. Talluri, G. Gonzalez, M. Fulciniti, J. M. Karp, R. H. Prabhalla, R. Karnik, *Sci. Rep.*, **2017**, *7*, 45681.

[20] Y. Liu, T. Germain, D. Pappas, *Anal. Bioanal. Chem.*, **2014**, *406*, 7867.

[21] N. T. Huang, W. Chen, B. R. Oh, T. T. Cornell, T. P. Shanley, J. Fu, K. Kurabayashi, *Lab Chip*, **2012**, *12*, 4093.

[22] C. H. Chu, R. Liu, T. Ozkaya-Ahmadov, M. Boya, B. E. Swain, J. M. Owens, E. Burentugs, M. A. Bilen, J. F. McDonald, A. F. Sarioglu, *Lab Chip*, **2019**, DOI: 10.1039/C9LC00575G

[23] D. A. L. Vickers, E. J. Chory, S. K. Murthy, *Lab Chip*, **2012**, *12*, 3399.

[24] W. H. Coulter, *Proc. Natl. Electron. Conf.*, **1956**, *12*, 1034.

[25] R. W. DeBlois, C. P. Bean, *Rev. Sci. Instrum.*, **1970**, *41*, 909.

[26] N. N. Watkins, U. Hassan, G. Damhorst, H. Ni, A. Vaid, W. Rodriguez, R. Bashir, *Sci. Trans. Med.*, **2013**, *5*, 214ra170.

[27] U. Hassan, R. Zhu, R. Bashir, *Lab Chip*, **2018**, *18*, 1231.

[28] E. Valera, J. Berger, U. Hassan, T. Ghonge, J. Liu, M. Rappleye, J. Winter, D. Abboud, Z. Haidry, R. Healey, N. T. Hung, N. Leung, N. Mansury, A. Hasnain, C. Lannon, Z. Price, K.

White, R. Bashir, *Lab Chip*, **2018**, *18*, 1461.

[29] U. Hassan, T. Ghonge, B. Reddy Jr., M. Patel, M. Rappleye, I. Taneja, A. Tanna, R. Healey, N. Manusry, Z. Price, T. Jensen, J. Berger, A. Hasnain, E. Flaugher, S. Liu, B. Davis, J. Kumar, L. White, R. Bashir, *Nat. Comm.*, **2017**, *8*, 15949.

[30] R. Liu, N. Wang, F. Kamili, A. F. Sarioglu, *Lab Chip*, **2016**, *16*, 1350.

[31] N. Wang, R. Liu, A. F. Sarioglu, *J. Visualized Exp.*, **2017**, *121*, e55311.

[32] R. Liu, W. Waheed, N. Wang, O. Civelekoglu, M. Boya, C. H. Chu, A. F. Sarioglu, *Lab Chip*, **2017**, *17*, 2650.

[33] R. Gold, *IEEE Trans. Inf. Theory*, **1967**, *13*, 619.

[34] R. Gold, *IEEE Trans. Inf. Theory*, **1968**, *14*, 154.

[35] R. Liu, N. Wang, N. Asmare, A. F. Sarioglu, *Biosens. Bioelectron.*, **2018**, *120*, 30.

[36] C. Cozens-Roberts, D. A. Lauffenburger, J. A. Quinn, *Biophys. J.*, **1990**, *58*, 841.

[37] Y. Zhang, V. Lyons, D. Pappas, *Electrophoresis*, **2018**, *39*, 732.

[38] M. A. Ingersoll, R. Spanbroek, C. Lottaz, E. L. Gautier, M. Frankenberger, R. Hoffmann, R. Lang, M. Haniffa, M. Collin, F. Tacke, A. J. R. Habenicht, L. Zieler-Heitbrock, G. J. Randolph, *Blood*, **2011**, *115*, e10.

[39] H. Schneck, B. Gierke, F. Uppenkamp, B. Behrens, D. Niederacher, N. H. Stoecklein, M. F. Templin, M. Pawlak, T. Fehm, H. Neubauer, *PLoS ONE*, **2015**, *10*, e0144535.

[40] J. Yoon, A. Terada, H. Kita, *J. Immunol.*, **2007**, *179*, 8454.

[41] G. Del Poeta, L. Maurillo, A. Venditti, F. Buccisano, A. M. Epiceno, G. Capelli, A. Tamburini, G. Suppo, A. Battaglia, M. I. Del Principe, B. Del Moro, M. Masi, S. Amadori, *Blood*, 2001, **98**, 2633.

[42] M. Schneider, V. Schumacher, T. Lischke, K. Lücke, C. Meyer-Schwesinger, J. Velden, F. Koch-Nolte, H.W. Mittrücker, *PLoS ONE*, **2015**, *10*, e0126007.

[43] T. Hernández-Caselles, M. Martínez-Esparza, A. B. Pérez-Oliva, A. M. Quintanilla-

Cecconi, A. García-Alonso, D. M. R. Alvarez-López, P. García-Peñarrubia, *J. Leukoc. Biol.*, **2006**, *79*, 46.

[44] F. Naeim, P. N. Rao, S. X. Song, W. W. Grody, *Atlas of Hematopathology*, Academic Press, Cambridge, MA, USA **2013**.

[45] S. P. Perfetto, P. K. Chattopadhyay, M. Roederer, *Nat. Rev. Immunol.*, **2004**, *4*, 648.

[46] I. J. Conlon, G. A. Dunn, A. W. Mudge, M. C. Raff, *Nat. Cell Biol.*, **2001**, *3*, 918.

[47] K. C. Cheung, M. Di Berardino, G. Schade-Kampmann, M. Hebeisen, A. Pierzchalski, J. Bocsi, A. Mittag, A. Tárnok, *Cytometry A*, **2010**, *77A*, 648.

[48] N. Wang, R. Liu, N. Asmare, C. H. Chu, A. F. Sarioglu, *Lab Chip*, **2019**, *19*, 3292.

[49] Z. Chen, T. Dodig-Crnković, J. M. Schwenk, S. Tao, *Clin. Proteom.*, **2018**, *15*, 7.

[50] B. B. Haab, *Proteomics*, **2003**, *3*, 2116.

[51] L. Diéguez, M. A. Winter, K. J. Pocock, K. E. Bremmell, B. Thierry, *Analyst*, **2015**, *140*, 3565.

**An electrically-readable microfluidic antibody microarray for the combinatorial immunophenotyping of cell populations** is demonstrated. The cell capture statistics across the whole device is acquired from a single electrical output without any loss of information. The ability to electrically screen cell immunophenotypes on a disposable microfluidic chip could be transformative in cell-based diagnostics at the point-of-care and resource-limited scenarios.

**Keyword** microfluidics, microarray, immunophenotyping, flow cytometry, complete blood count

Ruxiu Liu, Chia-Heng Chu, Ningquan Wang, Tevhide Ozkaya-Ahmadov, Ozgun Civelekoglu, Dohwan Lee, A K M Arifuzzman, A. Fatih Sarioglu*

**Combinatorial immunophenotyping of cell populations with an electronic antibody microarray**

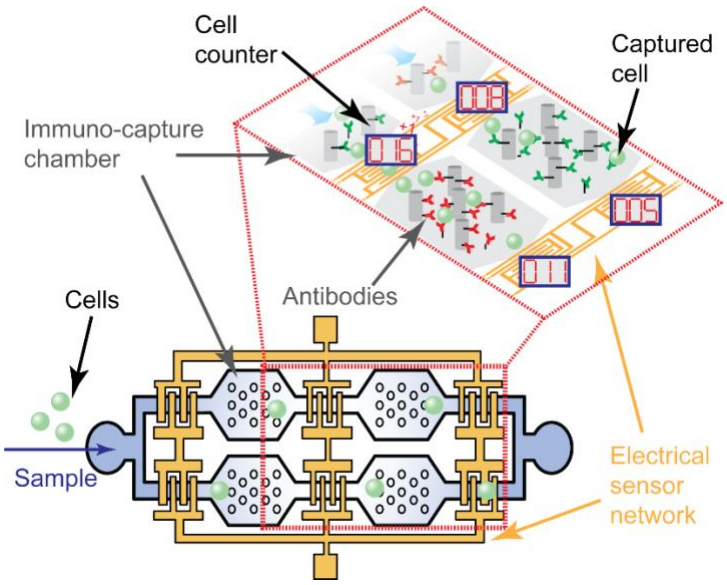

# Supporting Information

**Combinatorial immunophenotyping of cell populations with an electronic antibody microarray**

*Ruxiu Liu, Chia-Heng Chu, Ningquan Wang, Tevhide Ozkaya-Ahmadov, Ozgun Civelekoglu, Dohwan Lee, A K M Arifuzzman, A. Fatih Sarioglu**

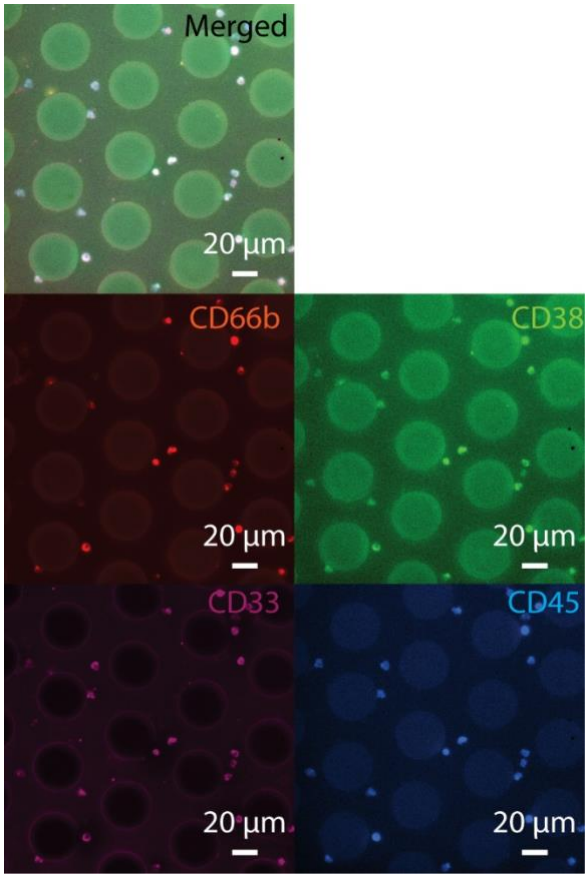


**Figure S1.** Immunofluorescence characterization of cell populations captured in microfluidic chambers. These representative fluorescence images show a group of leukocytes captured in the microfluidic chamber functionalized with anti-CD33 antibody. The captured cells were post-labeled with a cocktail of Alexa Fluor 594 anti-CD66b, Alexa Fluor 488 anti-CD38, Alexa Fluor 647 anti-CD33, and Brilliant Violet 421 anti-CD45 antibodies. Similar images were also taken in other capture chambers by scanning fluorescence microscopy. Finally, by counting the cells positive in each fluorescence channel, the frequency of different immunophenotypes was calculated for each capture chamber.

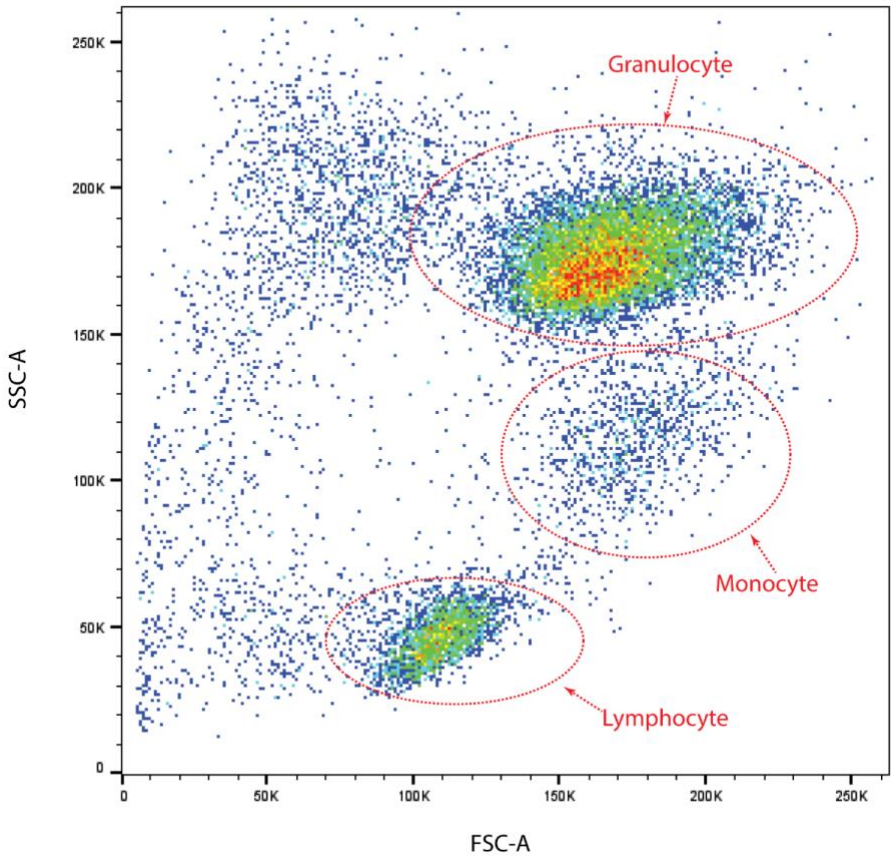


**Figure S2.** The FSC-SSC scatter plot obtained from the flow cytometry analysis of the leukocytes used in our study. Gates we used for designating leukocyte subpopulations are shown on the plot.

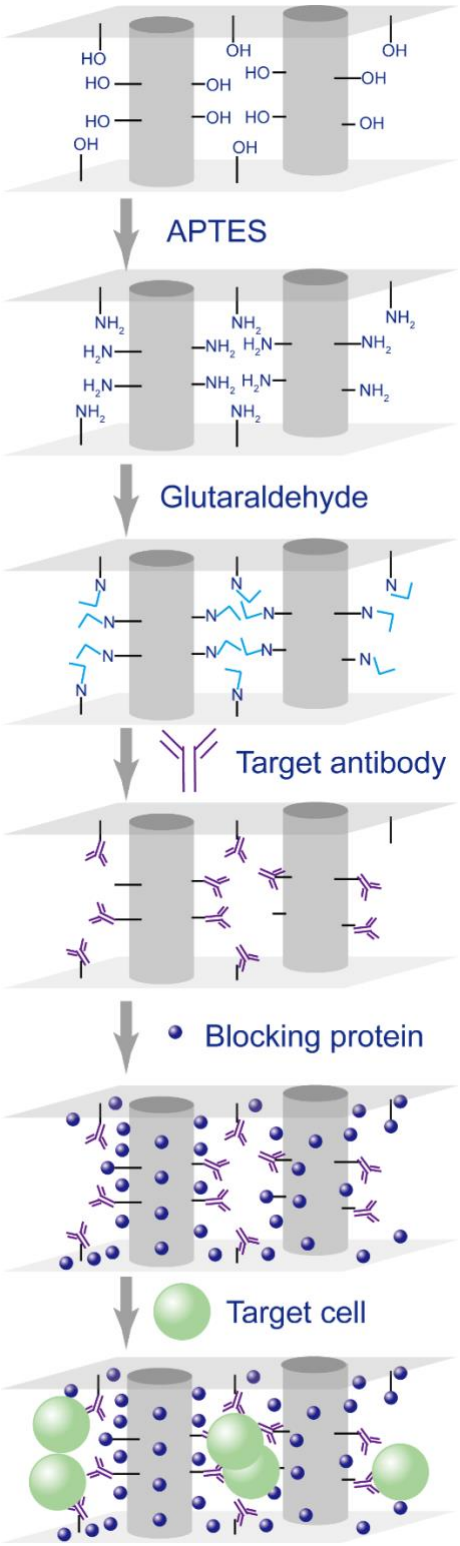


**Figure S3.** A schematic showing the step-by-step functionalization process and specific chemistry used to immobilize antibodies on the device surface.